PCCP

Enhancement of oil flow in shale nanopores by manipulating friction and viscosity

Journal:	*Physical Chemistry Chemical Physics*
Manuscript ID	CP-ART-04-2019-001960.R1
Article Type:	Paper
Date Submitted by the Author:	26-Apr-2019
Complete List of Authors:	Ho, Tuan; Sandia National Laboratories, Geochemistry Wang, Yifeng; Sandia National Laboratories

Enhancement of oil flow in shale nanopores by manipulating friction and viscosity

Tuan A. Ho[1]* and Yifeng Wang[2]

[1] *Geochemistry Department, Sandia National Laboratories, Albuquerque, New Mexico 87185, USA.*

[2] *Nuclear Waste Disposal Research and Analysis Department, Sandia National Laboratories, Albuquerque, New Mexico 87185, USA.*

*corresponding author:taho@sandia.gov

Abstract

Understanding the viscosity and friction of a fluid under nanoconfinement is key to nanofluidic research. Existing work on nanochannel flow enhancement has been focused on simple systems with only one to two fluids considered such as water flow in carbon nanotube, and large slip length have been found to be the main factor for the massive flow enhancement. In this study, we use molecular dynamics simulations to study the fluid flow of a ternary mixture of octane-carbon dioxide-water confined within two muscovite and kerogen surfaces. The results indicate that, in a muscovite slit, supercritical CO_2 ($scCO_2$) and H_2O both enhance the flow of octane due to (i) a decrease in the friction of octane with the muscovite wall because of the formation of thin layers of H_2O and $scCO_2$ near the surfaces; and (ii) an reduction in the viscosity of octane in nanoconfinement. Water reduces octane viscosity by weakening the interaction of octane with muscovite surface, while $scCO_2$ reduces octane viscosity by weakening both octane-octane and octane-surface interactions. In a kerogen slit, water does not play any significant role in changing the friction or viscosity of octane. In contrast, $scCO_2$ reduces both the friction and the viscosity of octane, and the enhancement of octane flow is mainly caused by the viscosity reduction. Our results highlight the importance of multicomponent interactions in nanoscale fluid transport. The results presented here also bear a direct implication to enhanced oil recovery in unconventional reservoirs.

Introduction

Nanoscale fluid flow plays an important role in many applications including water desalinization,[1] energy conversion,[2, 3] and shale oil/gas production.[4, 5] One challenge in nanofluidic research is to understand the impact of molecular interactions on the collective properties (e.g., flow rate).[6, 7] Such knowledge is necessary in the bottom-up approach to design nanofluidic devices. Nanoscale fluid transport can be very different from a macroscopic flow. For example, a macroscopic flow in a cylindrical tube is described by a no-slip boundary condition (i.e., the velocity of the fluid diminishes at the wall) Hagen-Poiseuille (HP) equation:

$$Q_{no-slip} = {\pi r^4 \Delta P}/{8\mu L} \quad (1)$$

where r is the pore radius, μ is the fluid viscosity, ΔP/L is the pressure drop along the channel length L, and $Q_{no-slip}$ is the flow rate. In a nanochannel, no-slip boundary condition may no longer be held. Instead, the slip boundary condition (i.e., the interfacial fluid velocity is different from the wall velocity) has been observed and considered to be responsible for massive flow enhancement,[8-10] relative to the flow rate calculated using equation (1). The enhancement factor is defined as:[11, 12]

$$\varepsilon = \frac{Q_{slip}}{Q_{no-slip}} = (1 + \frac{8L_s}{2r}) \quad (2)$$

where L_s is the slip length defined as the extrapolated distance from the interface to where the fluid velocity vanishes. The slip length L_s can also be calculated as the ratio of the viscosity μ of the confined fluid and the friction coefficient λ:[11]

$$L_s = \mu/\lambda \quad (3)$$

Combining (1), (2) and (3), we have

$$Q_{slip} = ({\pi r^4 \Delta P}/{8\mu L})(1 + \frac{8\mu}{2r\lambda}) \quad (4)$$

As shown in equation (4), reducing friction coefficient λ will increase the slip length and thus enhance the flow rate. In general, low friction is observed on a hydrophobic surface while high friction is found on a hydrophilic surface.[13] The low friction of water flow in a hydrophobic channel [e.g., carbon nanotube (CNT)] is the result of the unfavorable interaction of CNT with

water.[14] To obtain low friction, one can also engineer a shear-free air-liquid interface between the original solid-liquid interface using hydrophobic chemistry combining with nano-scale topology control,[15] or using a molecular lubricant.[4]

Viscosity plays more complicated role in a nanoscale flow because it appears in both the denominator and the numerator of equation (4). Increasing viscosity, on the one hand, increases the L_s and thus enhances the flow rate. On the other hand, increasing viscosity decrease the $Q_{no\text{-}slip}$. Even though not easy to measure, the viscosity of a fluid confined in a nanochannel is known to be different from the corresponding bulk viscosity. For CNTs, conflicting results have been reported that the water viscosity increases,[16-18] and decreases[19] with respect to the pore diameter, and that water viscosity in graphite nanopore is higher than bulk water viscosity.[9] In a hydrophilic nanochannel, water viscosity dramatically increases compared to the bulk viscosity.[20, 21] Therefore, accounting for the effect of viscosity under confinement is vital to study flow enhancement in nanochannels.[9, 22] Unfortunately, many existing studies generally assume a bulk viscosity for a confined fluid.[8, 23-25]

In short, determining fluid viscosity and friction is prerequisite to understand nanoscale fluid flow. Most existing work in this research area has been focused on a single fluid system (e.g., water in a CNT),[26-28] in which the mechanism for flow enhancement is relatively well understood. The questions to be addressed in this study are: (1) can we can manipulate the friction and viscosity of a fluid in an existing nanochannel without changing the surface chemistry (as in current practice) to increase the flow rate; (2) if yes, what is the mechanism to reduce the friction and viscosity of the fluid in the nanopore? In the current work, we use molecular dynamics simulations to study the multicomponent interaction of octane, $scCO_2$, and H_2O in both inorganic (muscovite) and organic (kerogen) nanopores. Specifically, we focus on the effects of $scCO_2$ and/or H_2O on the friction and viscosity of octane the nanopores and consequently on the octane flow enhancement. The analysis will provide an insight into the molecular origin of flow enhancement in complex systems.

Method

Simulation systems

As mentioned above, two types of geological porous materials were studied: (i) inorganic materials represented by muscovite (i.e. denoted as M) and (ii) organic materials modeled by kerogen (denoted as K). Different pore fluids including octane (i.e., denoted as O), H_2O, and $scCO_2$ were

placed in a muscovite or kerogen nanopore. For example, label M_O_CO_2_H_2O means a mixture of octane, scCO_2, and H_2O is in a muscovite nanopore. Label K_O_H_2O means both octane and H_2O present in a kerogen nanopore. Figure 1 shows simulation snapshots for M_O_CO_2_H_2O (A) and K_O_CO_2_H_2O (B) systems. Table 1 reports all systems considered in this work and the number of octane, H_2O, and scCO_2 molecules simulated in each system. In the muscovite pore, the number of water molecules is determined based on the monolayer configuration near the interface. The number of CO_2 molecules is large enough (i.e., more than twice of the number of octane molecules) so that it has a significant impact on the viscosity and friction coefficient of octane with surfaces. At the beginning of the simulation, fluids were placed near a solid surface (i.e., kerogen or muscovite). When applying periodic boundary condition in all directions, the fluid becomes confined in a nanopore in the z direction. The confinement pressure (i.e., 200 atm) was obtained by running the simulation in NPT (constant number of particles, pressure, and temperature) ensemble. The pressure was coupled in z direction and temperature was kept constant at 300K.

Table 1. Simulated systems and number of octane, H_2O, and CO_2 molecules for each system.

	Muscovite nanopore				Kerogen nanopore			
	M_O	**M_O_H_2O**	**M_O_CO_2**	**M_O_CO_2_H_2O**	**K_O**	**K_O_H_2O**	**K_O_CO_2**	**K_O_CO_2_H_2O**
Octane	1125	1125	1125	1125	1125	1125	1125	1125
H_2O		2350		2350		3094		3094
CO_2			2512	2512			2470	2470

Muscovite was selected because it has a similar mineral structure to illite, a common clay mineral found in a shale oil/gas reservoir.[29] Kerogen is the carbon material responsible for oil and gas generation, storage, and transport in oil/gas reservoirs. In our previous work,[4, 5, 30, 31] we simulated an over-mature kerogen to study the interaction of organic matter with shale gas. In this work, we use immature kerogen model (i.e., IIB) developed by Ungerer et al.[32] to investigate the interaction of organic matter with shale oil. The immature kerogen model shown in Fig. 1C has the formula of $C_{234}H_{263}O_{14}N_5S_2$, which matches the experimentally observed H/C, O/C, S/C and N/C ratios.

Kerogen surface construction

The size of the kerogen surface is 89.67x103.66x18.32 $Å^3$. To build the kerogen surface, we applied the same strategy used in our previous work.[4] We first placed 32 kerogen molecules on

top of a muscovite surface in a box with dimensions of 89.67x103.66x200.40 $Å^3$. The size of the muscovite substrate is 89.67x103.66x18.68 $Å^3$. The kerogen was initially mixed up in a NVT (constant number of atoms, volume, and temperature) simulation in which the temperature was reduced from 1000 K to 300 K in 100 ps with 1 fs time step. For this simulation, we only considered short-range Lennard-Jones (LJ) interaction with a cut-off distance of 5 Å, and the muscovite surface was kept rigid. In addition, to quickly obtain the desired kerogen density the simulation box was deformed every 100 steps so that the final box size in the z direction was 39 Å after 100 ps (the initial box size in z direction was 200.4 Å).

Next, the system was equilibrated in a NVT ensemble simulation for 100 ps. The temperature was kept constant at 300 K. During this simulation, the Lennard-Jones cutoff was 10 Å and the long-range electrostatic interactions were calculated using the PPPM (particle-particle-particle-mesh) solver.[33] All kerogen and muscovite atoms were free to move during the course of the simulation. In the final step, the whole system was equilibrated in a NPT simulation for 2 ns. The pressure (1 atm) was controlled in z direction. The final configuration of the simulation system is shown in Fig. 1D. The box size in the z direction is 40.30 Å including 18.68 Å of muscovite surface. The calculated kerogen density is 1.10 g/cm^3, which is in agreement with experimental data.[32] Note that we used LJ cut-off of 5 Å to initially mix up the kerogen molecules in the NVT simulation. If we used LJ cut-off of 10Å, the kerogen molecules quickly aggregate and it becomes impossible to compress the kerogen structure to the constrained density of 1.10 g/cm^3. In the subsequent simulations, we used LJ cut-off of 10Å to make sure that interaction of a kerogen molecule with other molecules are correctly calculated. After removing the muscovite surface, a kerogen/vacuum interface was obtained and used to build the simulation system described in Fig. 1B.

Flow simulation

The flow of fluid inside a muscovite or kerogen nanochannel was driven by a body force (i.e., an acceleration of 3×10^{-4} Kcal/Å.g or $\sim12.55\times10^{12}$ m/s^2) added to all octane molecules (and only to octane molecules) in the x direction. The flow simulation was carried out for 15 ns in the NVT ensemble. During the flow simulation, a few atoms belonging to the muscovite or kerogen surface was excluded from the integration of the equation of motion to keep the kerogen surface stationary (i.e., the velocity of kerogen and muscovite surface is zero). All other atoms were free to move. In our previous work[31] we have shown that kerogen can expand its initial volume up to 11% in 200

atm CO_2 environment. Since the majority of kerogen atoms are free to move to some extent in the simulation presented in this work, we expect that the kerogen surface can deform. However, it is challenging to quantify the deformation of the kerogen surface because of the rough interface. In a MD simulation, the acceleration is on the order of 10^{11}-10^{12} m/s^2,[34, 35] so that the noise from the thermal motion can be avoided (with the limitation of the computational resources).[36] In our simulation the applied acceleration is slightly higher than that in the literature due to the surface roughness[37] and likely high confined pressure (200atm) in the z direction. In the flow simulation, two approaches are usually used to control the temperature: the thermostat is connected to all atoms in the system, and the thermostat is coupled only to the surfaces.[38] In the latter case, the confined fluid molecules exchange heat with the wall during the course of the simulation.[39] For the former case only the velocity component perpendicular to the flow direction is usually thermostatted.[40] In our simulations, as the flow velocity is very small compared to the thermal velocity, we thermostat all fluid atoms in the system and include the flow velocity in our temperature calculations. This will not result in significant error because a small flow velocity contributes only a tiny fraction of the total kinetic energy.[41, 42]

Force field and simulation parameters

In our simulations, muscovite was simulated by ClayFF force field.[43] Kerogen and octane was modeled by CVFF force field.[44] Kerogen and octane force field assignment is performed using Material Studio.[45] Water molecules were simulated using the flexible SPC water model.[46] The CO_2 molecules were simulated as a 3-site rigid model by the TRaPPE force field.[47] The rigidity of the CO_2 molecule was maintained by using the algorithm proposed by Kamberaj.[48] Interactions among un-like atoms were calculated using the Lorentz-Berthelot mixing rules $\varepsilon_{ij} = \sqrt{\varepsilon_{ii}\varepsilon_{jj}}$ and $\sigma_{ij} = (\sigma_{ii} + \sigma_{jj})/2$, where ε and σ are the depth of the potential energy well and the distance at which the inter-particle Lennard-Jones potential is zero, respectively. If not specified the long-range electrostatic interactions were calculated using the PPPM (particle-particle-particle-mesh) solver.[33] Periodic boundary condition is applied in all directions. Temperature and pressure were controlled using the Nose-Hoover scheme.[49, 50]

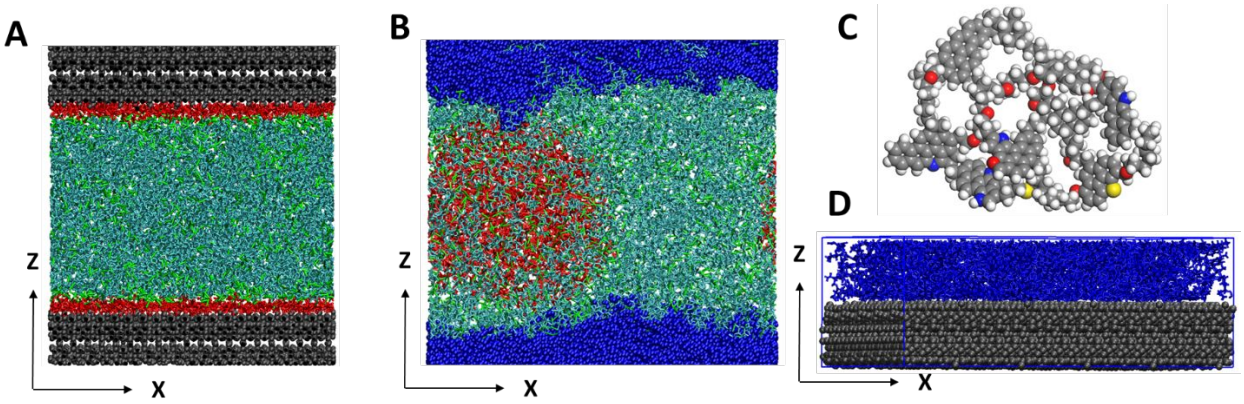

Figure 1. Simulation snapshot demonstrates water (red), scCO$_2$ (green), and octane (cyan) confined in muscovite (gray) (A) and kerogen (blue) (B) nanopores. Molecular structure of immature kerogen (C). Silver, white, red, blue, and yellow spheres represent carbon, hydrogen, oxygen, nitrogen, and sulfur atoms, respectively. Simulation snapshot illustrates the kerogen/muscovite system used to construct a kerogen surface (D).

Results and discussion

Flow in a muscovite nanopore

In Fig. 2 A we present the density profiles of octane in the muscovite nanopore. The results indicate that when H_2O and/or $scCO_2$ coexist with octane, the structural properties of octane severely alter. For example, when only octane is in the pore (i.e., M_O system) the density profile evidences the formation of multiple octane layers across the pore. When water is added to the system (i.e., M_O_H_2O system), water adsorbs onto the muscovite surface (Fig. 1A). Multiple layers of octane are still observed with reduced peak intensity, compared to the M_O system. The water and octane structure in M_O_H_2O system is constant with the contact angle results of water and oil on muscovite surface studied previously.[51, 52]

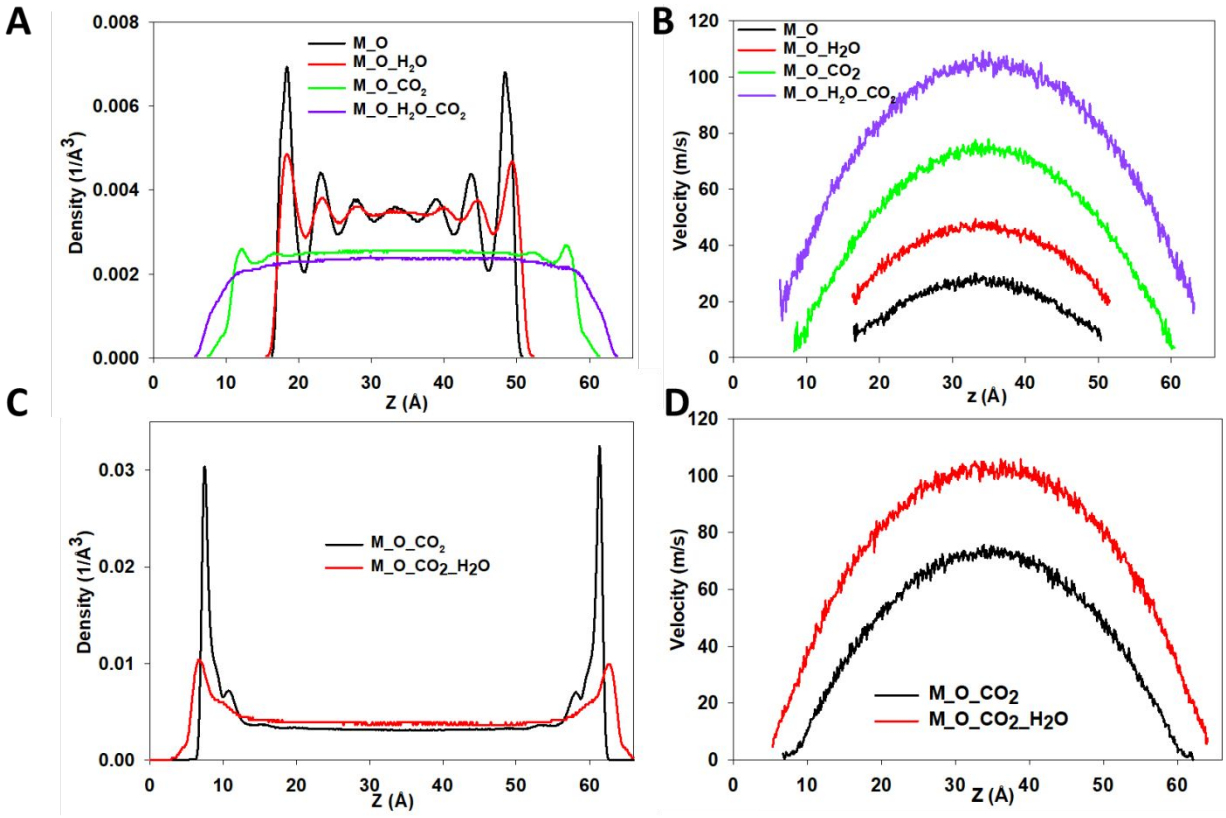

Figure 2. Density (A) and velocity (B) profiles of octane in the muscovite nanopore. Density (C) and velocity (D) profiles of CO_2 in the muscovite nanopore.

When $scCO_2$ and octane coexist in the muscovite nanopore (M_O_CO_2 system), the density profile indicates that octane evenly distributes in the nanopore with small peaks observed at the interface (Fig. 2A). CO_2 molecules form dense layers near the muscovite interfaces (black line, Fig 2C). Note that $scCO_2$ and octane are miscible, thus reducing the density of octane across the pore as compared to a M_O or M_O_H_2O system. When octane, H_2O, and $scCO_2$ are all present in the pore (i.e., M_O_CO_2_H_2O), there is no octane peak observed on the density profile (Fig. 2A). Octane uniformly distributes across the nanopore. Because of the adsorption of water at the interface (Fig. 1A), the intensity of the CO_2 peak on the CO_2 density profile for the M_O _CO_2_H_2O system is significantly reduced, compared to that in the M_O_CO_2 system (Fig. 2C).

The changes in the chemical profiles as noticed in Fig. 2A and 2C in the presence of $scCO_2$ and/or H_2O greatly alter the hydrodynamics of octane flow. The velocity profile (Fig. 2B) of octane in the muscovite nanopore (M_O system) indicates that at the interface (defined as the location where the octane density equals 10% of the octane density in the middle of the pore) octane flows with a slip velocity of ~7 m/s. When water is present (M_O_H_2O system), water forms a thin molecular

layer between the octane and the muscovite, which enhances the slip velocity of octane to ~21 m/s. The water induced flow enhancement factor, $\frac{Q_{\text{M\_O\_H}_2\text{O}}}{Q_{\text{M\_O}}}$, is calculated to be ~1.95, where Q_α is the octane flow rate of the α (i.e., M_O or M_O_H_2O) system calculated by integrating the octane velocity profile. Note that when adding H_2O to the M_O system, the pore size is bigger. However, because we simulate the same number of octane molecules, the volumetric flow rate does not depend on the pore size. The flow enhancement obtained when water is added is partly because of the larger slip length (i.e.,10.2 ± 0.43 Å) of octane flow in the M_O_H_2O system, compared to that (i.e., 5.3 ± 0.2 Å) of octane flow in the M_O system (the slip length is determined with the method reported in our previous work[4]). Note that water and octane are immiscible. Therefore, in a bulk system, adding water should not affect the viscosity of octane. As discussed later, however, our simulations show that the flow enhancement is also partly due to the reduction of octane viscosity by the presence of a thin water film at the pore surface.

When $scCO_2$ is present (M_O_CO_2), the velocity profile of $scCO_2$ (Fig. 2D) shows no-slip for CO_2 flow at the boundary, while octane flow exhibits a small slip on a dense layer of $scCO_2$ formed near the surface (slip velocity ~ 2 m/s, Fig. 2B). The slip length calculated for octane flow in the M_O_CO_2 system is 1.04 ± 0.03 Å. The enhancement factor $\frac{Q_{\text{M\_O\_CO}_2}}{Q_{\text{M\_O}}}$ is ~3.84. Here we do not directly compare the slip length and slip velocity of the octane-$scCO_2$ mixture with those of pure octane in the muscovite nanopore because the octane-$scCO_2$ mixture and pure octane are two fluids with different viscosity and density. The conclusion to be drawn here is that adding $scCO_2$ into the M_O system enhances the flow of octane in the muscovite nanopore. One known reason for this observation is that the viscosity of the bulk octane-$scCO_2$ mixture, is lower than that of bulk octane. Now the question is how the viscosity of the octane-$scCO_2$ mixture changes under nanoconfinement, and if the friction coefficient of octane with the pore surface changes upon the introduction of $scCO_2$ into the M_O system (see a later discussion).

In the M_O_CO_2_H_2O system, the slip length of octane flow is 3.7 ± 0.3 Å, which is larger than that for M_O_CO_2 system. The enhancement factor is $\frac{Q_{\text{M\_O\_CO}_2\text{\_}H_2O}}{Q_{\text{M\_O\_CO2}}}$ ~ 1.65, indicating the effect of water on the flow of the octane-$scCO_2$ mixture. One obvious reason is the increase of the slip length of the octane-$scCO_2$ mixture flow on the water layer. The remaining question is if the viscosity of the octane-$scCO_2$ mixture changes when water is added to the M_O_CO_2 system (see

a later discussion). For enhanced oil recovery, adding both $scCO_2$ and H_2O into inorganic nanopore significantly enhances the oil flow by a factor of $\frac{Q_{M\_O\_CO_2\_H_2O}}{Q_{M\_O}}$ (~ 6.37).

In Figure 3, we report the friction coefficient and the viscosity of fluids in a muscovite nanopore, to provide an overall explanation for the enhancement of octane flow, as well as to suggest a possible mechanism to alter the friction and viscosity of a fluid in nanopores in general. The friction coefficient λ is determined as:[14, 53] $\lambda = \frac{1}{2Ak_BT}\int_0^\infty dt\langle F_x(t)F_x(0)\rangle$, where A is the surface area, k_B is the Boltzmann constant, T is the temperature, and $F_x(t)$ is the total force of the fluid acting on the wall in the x direction obtained from equilibrium simulations (i.e., not in flow simulations), and factor '*2*' accounts for two interfaces in our simulation box. In Fig. 3A, we report the friction coefficient calculated for octane in a muscovite pore. In this calculation, only the force F_x from octane acting on the surface is considered even if H_2O and $scCO_2$ are present in the pore. The results indicate that the friction coefficient of octane on the surface reduces significantly when H_2O or/and $scCO_2$ is added. Water appears to be more effective to reduce the friction of octane with the surface, than $scCO_2$ (i.e., compare M_O_H_2O with M_O_CO_2). Water prevents the direct contact of octane with the muscovite surface (Fig. 1A), thus greatly reducing the friction coefficient of octane. Similarly, $scCO_2$ also forms a thin interfacial layer (Fig. 2C), which also reduces the friction of octane with the surface. When both $scCO_2$ and H_2O are present (M_O_CO_2_H_2O), the friction coefficient of octane with the surface is comparable with that of the system with only water present (M_O_H_2O).

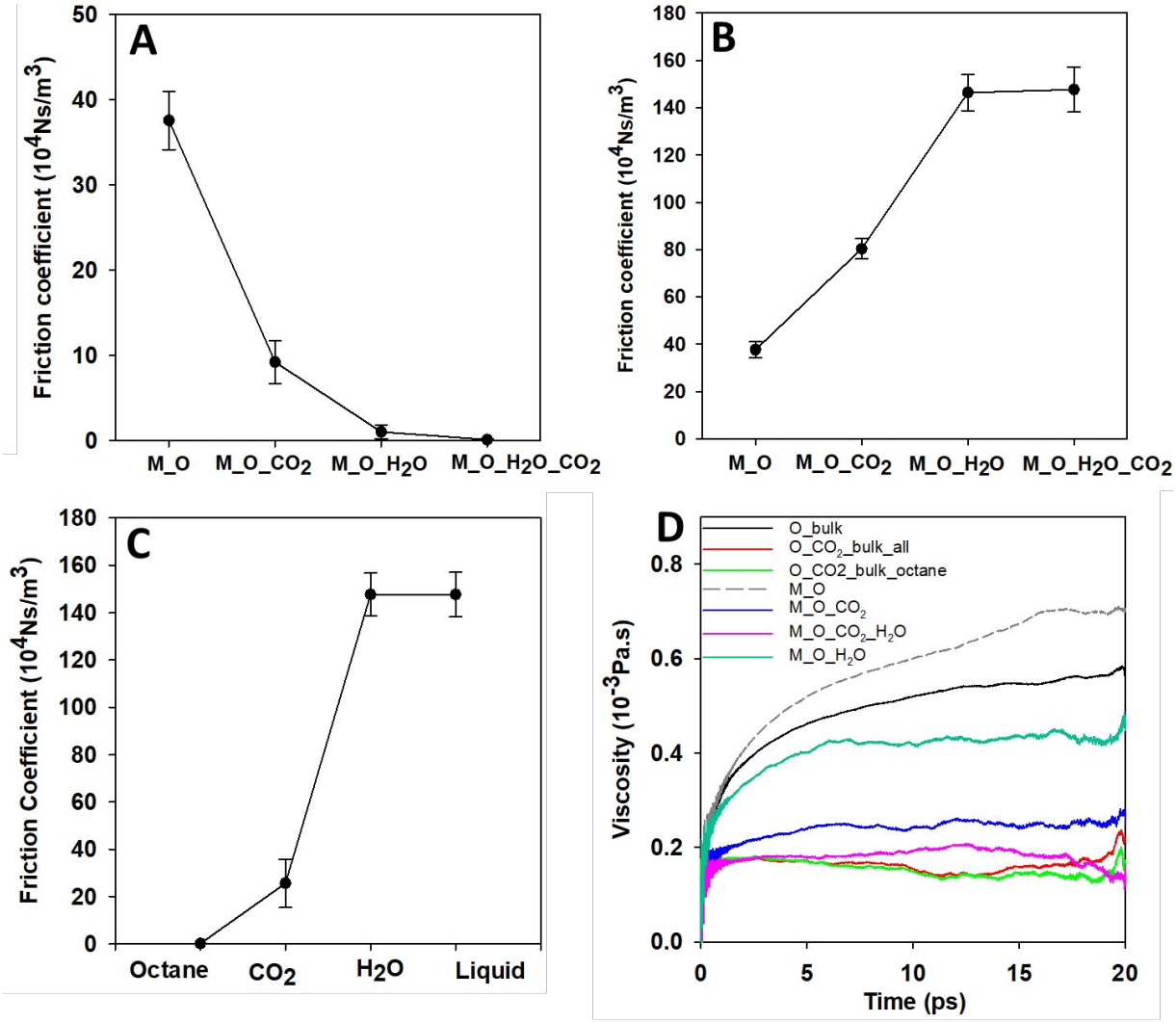

Figure 3. Friction coefficient of octane (A) in the muscovite pore. Friction coefficient of liquid (B) calculated for all fluid components present in the muscovite pore. Friction coefficient calculated for each fluid component in the M_O_CO_2_H_2O system (C). Viscosity of octane, and octane-scCO_2 mixture in bulk and in muscovite pore at temperature of 300 K and pressure of 200 atm (D).

In Figure 3B, we present the friction coefficient of liquid with the muscovite surface. In this calculation, the force acting on the wall, *Fx*, is calculated for all liquid components in the nanopore. For example, in the M_O_CO_2_H_2O system, *Fx* is the sum of forces acting on the wall in the x direction from octane, scCO_2, and H_2O. The results indicate that adding scCO_2 and H_2O into the nanopore increases the friction of liquid with the wall because H_2O and scCO_2 strongly interacts with the surface. The results also indicate that adding scCO_2 to the M_O_H_2O system does not

change the friction coefficient of fluid with surface (i.e., M_O_H_2O vs. M_O_H_2O_CO_2), because the friction of H_2O with the surface dominates the friction calculated for the liquid. The contribution of each fluid component (i.e., octane, H_2O and $scCO_2$) to the friction coefficient of the liquid with the wall for the M_O_H_2O_CO_2 system is reported in Fig. 3C. The results confirm that H_2O has the highest friction coefficient among the fluid components considered.

As discussed earlier, the viscosity of a fluid under nanoconfinement needs to be taken into account to understand a fluid flow in a nanopore. We now investigate (i) how the viscosity of an octane-$scCO_2$ mixture changes under nanoconfinement and (ii) whether adding H_2O to octane would modify the oil viscosity in a nanopore even the two components are immiscible. The viscosity is calculated by integrating stress-stress correlation functions:$\mu = \frac{V}{k_B T}\int_0^\infty dt\langle P_{xy}(t)P_{xy}(0)\rangle$, where V is the volume of fluid, k_B is the Boltzmann constant, T is the temperature, P_{xy} is the xy stress component obtained from equilibrium simulation.[54] The stress P_{xy} is recorded every 2fs (time step 1fs). The correlation function is calculated for 20ps. In some systems, the simulation was conducted for 5ns to obtain a constant viscosity as a function of correlation time (i.e., Fig. 3D). However, for the M_O, K_O, K_O_CO_2, K_O_H_2O, and K_O_CO_2_H_2O systems the simulation was carried out for 50ns. Despite of long simulation time, it is difficult to obtain a constant viscosity as a function of correlation time for a kerogen system (reported later). The reason is that octane and sCO_2 interact strongly with kerogen, and some octane and $scCO_2$ molecules adsorb deeply inside the kerogen structure. Therefore, we just qualitatively discuss the viscosity results in kerogen pore (discussed later) by comparing the trend of the viscosity as a function of correlation time for different cases.

For the bulk $scCO_2$-octane mixture, we calculate the viscosity in two ways and the results are comparable (red and green lines, Fig. 3D). In one way, we calculate P_{xy} for both octane and sCO_2 (i.e., the summation of P_{xy} for octane and $scCO_2$) and V is the volume of the simulation box. In another way, we consider Pxy only for octane and V is the volume of octane (assuming that the volume of octane in the octane-$scCO_2$ mixture equals the bulk volume of pure octane). This serves as a benchmark for the calculation of octane viscosity using only P_{xy} and V for octane when other fluids are present in the nanopore. The results indicate that under nanoconfinement, the viscosity of pure octane and of the octane-$scCO_2$ mixture increase, compared to the bulk viscosity (black

vs. grey lines; and red vs. blue lines, Fig. 3D). As expected, the viscosity of the $scCO_2$-octane mixture is smaller than that of pure octane, regardless of nanoconfinement.

Surprisingly, when adding water into the M_O system, the viscosity of octane (i.e., that of the M_O_H_2O system) becomes smaller than the bulk octane viscosity. Viscosity is the measure of the fluid resistance to an external force, and it depends on the fluid/fluid interaction. Because of the nanoconfinement, the fluid/fluid interaction in a nanopore is expected to be different from fluid/fluid interaction in the bulk. Such a difference rises the viscosity of octane in the muscovite pore, compared to the bulk viscosity. When adding water to the M_O system octane becomes confined within two 'water surfaces'. The octane/octane interaction in the 'water pore' is different from the octane/octane interaction in the bulk, and in the muscovite pore. We postulate that the highly unfavorable interaction of octane with the H_2O film decreases the viscosity of octane, compared to the bulk viscosity. This interaction could reduce the activation energy for molecule to move from one location to another, similar to the case of water in CNT.[18] Adding water to the M_O system decreases the viscosity of octane about ~1.5 times (cyan vs. grey lines). These results point to a possible mechanism to manipulate the viscosity of a fluid under nanoconfinement, that is, using an additive to intercalate a thin molecular layer between the fluid and the surface. As we discussed earlier, adding water to the M_O system decreases the friction coefficient of octane with the surface about 37 times. According to equation (3), the decreasing of friction coefficient dominates the reduction of viscosity when H_2O is added, resulting in the increasing of slip length. According the equation (1) decreasing viscosity also increases the flow rate. Therefore, adding water enhances the flow rate of octane in a muscovite nanopore (M_O vs. MO_H_2O) in two ways: increasing the slip length and decreasing the viscosity. A similar conclusion can also be drawn in comparison of the M_O_CO_2 with the M_O_CO_2_H_2O system, i.e., the viscosity of octane in M_O_CO_2_H_2O is ~1.25 times smaller than that of octane in the M_O_CO_2. The friction coefficient of octane in the M_O_CO_2_H_2O system is ~83 times smaller than that in the M_O_CO_2 system.

The results in Fig. 3D also suggest that the viscosity of octane in the M_O_H_2O system is higher than viscosity of octane in the M_O_CO_2 system (cyan vs. blue lines). Different from H_2O, $scCO_2$ changes viscosity of octane through two different mechanisms: (i) changing the interaction of octane with muscovite and (ii) changing the interaction between octane molecules (note that $scCO_2$

and octane are miscible). Therefore, $scCO_2$ is more effective to change the viscosity of octane in the nanopore, compared to water. This is the main reason for the higher octane flow rate for the M_O_CO_2 system as compared with the M_O_H_2O system (Fig. 2B), regardless of the fact that the friction coefficient of octane with the surface in the M_O_CO_2 is higher than that in M_O_H_2O system (Fig. 3A). In addition, the viscosity of octane in the M_O_CO_2_H_2O is smaller than that of octane in the M_O_H_2O system. This result helps understand the higher octane flow rate in M_O_CO_2_H_2O system, compared with the M_O_H_2O system, regardless of the comparable friction coefficient (considering the error bar) of octane with the surface for the two systems.

Flow in a kerogen nanopore

For a muscovite nanopore, the simulation results indicate that both $scCO_2$ and H_2O enhance the flow of octane. Two mechanisms are responsible for the enhancement: (i) the reduction of the friction of octane with the muscovite wall due to the formation of H_2O and $scCO_2$ layers near the surface; (ii) the reduction of the octane viscosity under nanoconfinement in the presence of the $scCO_2$ and H_2O layers. Water reduces the viscosity of octane by changing the interaction of octane with the muscovite surface, and $scCO_2$ reduces the viscosity of octane by changing the interactions of both octane with octane and octane with the surface. Compared to muscovite, kerogen is an organic material with a greater affinity to hydrocarbons, and less to water. Therefore, the behaviors of octane, $scCO_2$, and water are expected to be different from what we observed in a muscovite nanopore.

The first difference is that we do not observe multiple octane and $scCO_2$ layers on the density profiles (Fig 4A and C) because of kerogen surface roughness, compared to the muscovite surface. In addition, in the kerogen nanopore filled with octane and/or $scCO_2$ and water (i.e., K_O_H_2O and K_O_H_2O_CO_2 systems), water forms a spherical droplet (Fig. 1B). This result agrees with our previous report[4] that under $scCO_2$ atmosphere water does not wet the kerogen surface, although in the vacuum or air kerogen surfaces may become partially wetted. In practice, because water does not wet kerogen surface under high pressure condition of oil and $scCO_2$ we may not find water co-exist with $scCO_2$ and oil in the organic nanopore. However, we can perform the exercise under the assumption that kerogen is initially wet in the depleted oil and gas reservoir. When $scCO_2$ is pumped into the reservoir, for a short period of time $scCO_2$, water droplet, and oil can coexist until the water diffuses out of the pore. Because water forms a droplet in the middle of the kerogen

pore, it does not alter the velocity profiles of octane and $scCO_2$ (Fig. 4 B and D, K_O vs. K_O_H_2O, and K_O_CO_2 vs. K_O_CO_2_H_2O). When it is present, $scCO_2$ significantly increases the flow of octane (Fig. 4B, K_O vs. K_O_CO_2, K_O_H_2O vs. K_O_CO_2_H_2O). Note that the flow of octane and $scCO_2$ in all cases inhibits no-slip boundary conditions, indicating that $scCO_2$ and water do not change the hydrodynamics boundary condition of octane flow in the kerogen pore.

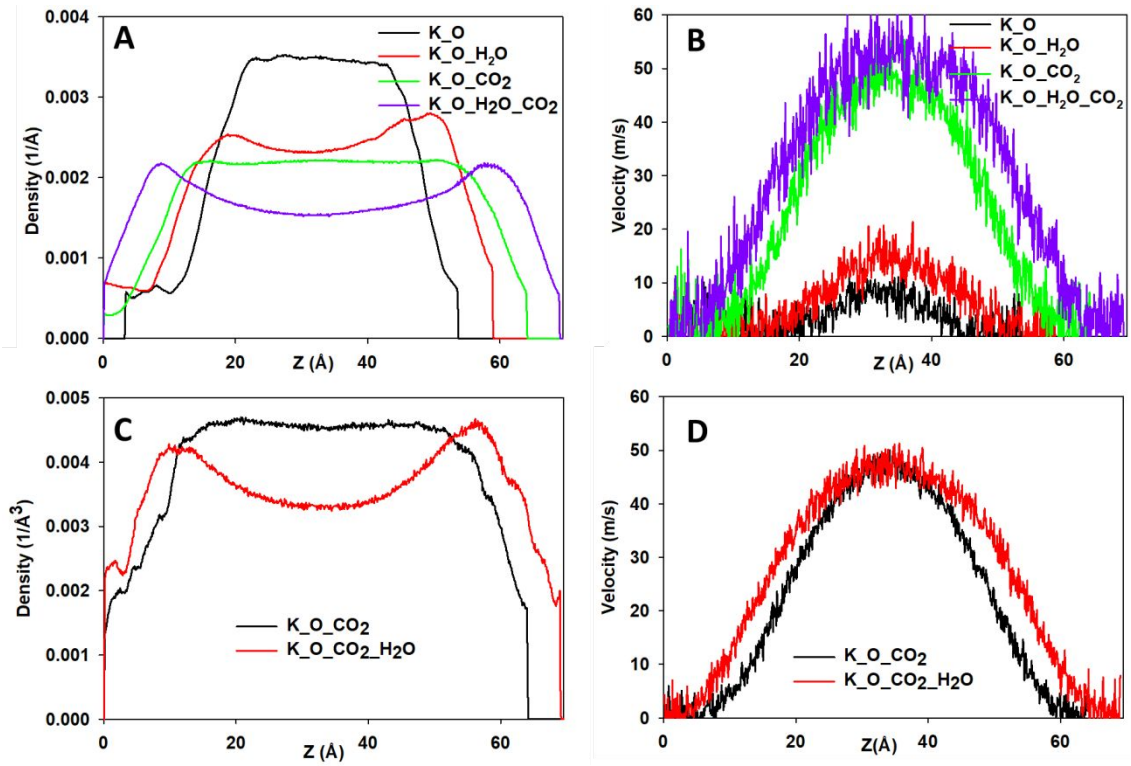

Figure 4. Density (A) and velocity (B) profiles of octane in muscovite nanopore. Density (C) and velocity (D) profiles of $scCO_2$ in muscovite nanopore.

In Figure 5A, we report the friction coefficient calculated for octane. The results indicate that water plays little impact on the friction of octane with the kerogen wall. The friction coefficient of octane in K_O_H_2O system is slightly smaller than that in K_O system, probably because the water droplet occupies a fraction of pore volume that reduces the surface area that octane contacts with the surface (inset of Fig. 5A). However, this effect is minimum (considering the errors bar). A similar conclusion can be obtained by comparing the friction of octane in the K_O_CO_2 system with that in the K_O_H_2O_CO_2 system.

In contrast to water, $scCO_2$ reduces the friction coefficient of octane by ~1.6 times (Fig 5.A, K_O vs. K_O_CO_2) because of the competitive adsorption with octane on the kerogen surface. However, the reduction in $scCO_2$ friction with the wall is not enough to change the slip length and the no-slip hydrodynamics boundary condition of octane flow. In other word, the reduction of the friction must be canceled out by the decrease of the viscosity (equation 3). In Figure 5B, we compare the friction coefficient of liquid. The friction coefficient of pure octane in the kerogen pore is comparable with that of the octane-water mixture (K_O vs. K_O_H_2O), in agreement with the conclusion that water plays a negligible role on the friction of octane with the kerogen pore. When $scCO_2$ is present, the friction coefficient of liquid increases, indicating a significant interaction of $scCO_2$ with kerogen. This observation is confirmed when decomposing the friction of liquid in the K_O_H_2O_CO_2 system into the friction of each fluid component as reported in Figure 5C. Accordingly, the friction of water with the surface is nearly zero, and the friction coefficients of $scCO_2$ and octane with kerogen are comparable.

In comparison with the results calculated for the muscovite pore, the friction coefficient of octane in the kerogen pore is much higher in all cases. This partly explains for the lower velocity of the octane in the kerogen nanopore, compared to the velocity of octane in the muscovite nanopore (Fig. 3B vs. Fig. 5B).

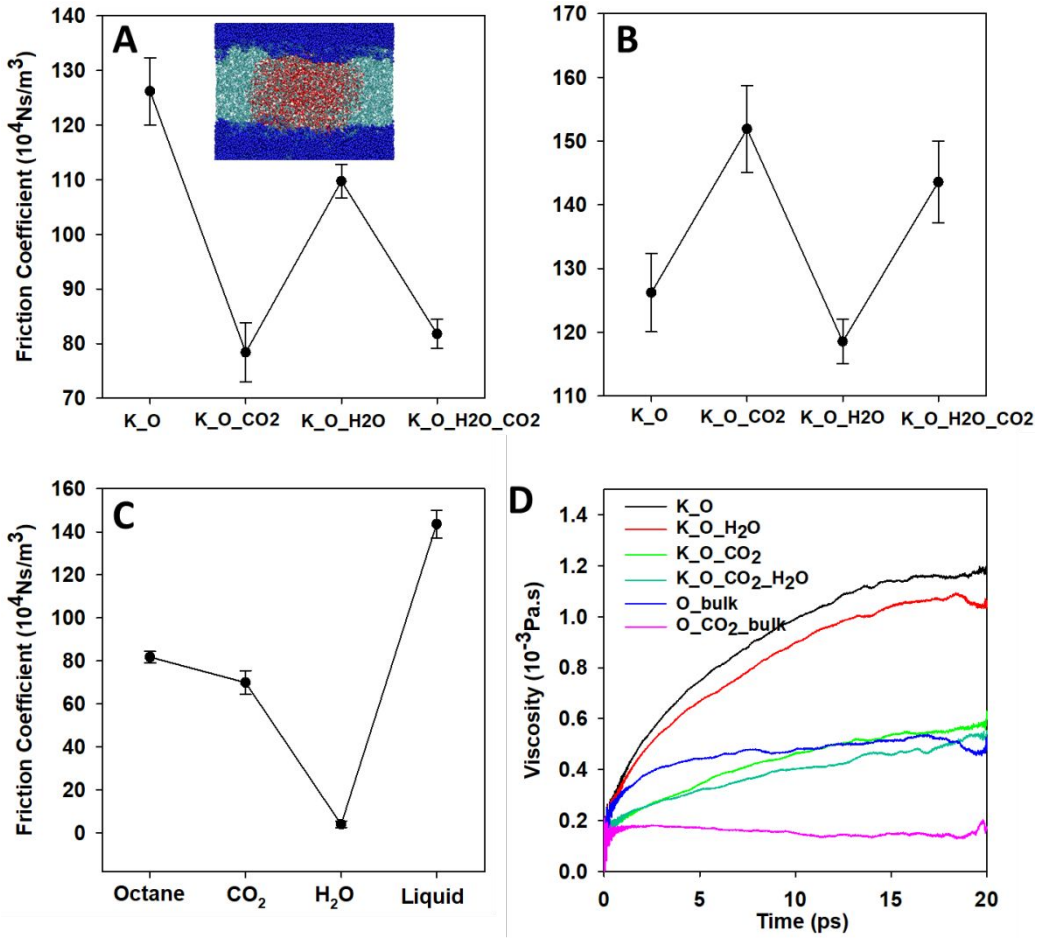

Figure 5. Friction coefficient of octane (A) in the kerogen pore. Inset: simulation snapshot demonstrating the K_O_H_2O system (see Fig. 1 for color code). Friction coefficient of liquid (B) calculated for all fluids present in the pore. Friction coefficient calculated for each fluid component in the K_O_CO_2_H_2O system (C). Viscosity of octane in the kerogen nanopore in the presence of both scCO_2 and H_2O (D).

In Fig. 5D, we report the viscosity of octane in the kerogen nanopore. The result indicates that the viscosity of pure octane (or the octane-scCO_2 mixture) in kerogen is higher than the bulk viscosity and also higher than those in the muscovite nanopore. This is due to the high affinity of octane and scCO_2 with kerogen. Combining with the friction coefficient result, we conclude that the friction coefficient and viscosity of octane in a kerogen nanopore are always higher than those in the muscovite nanopore. The results in Fig. 5D also indicate the minimum impact of water on the viscosity of octane in a nanopore (K_O vs. K_O_H_2O, and K_O_CO_2 vs. K_O_CO_2_H_2O). When scCO_2 is added into the K_O system, the viscosity of octane is reduced. Because both the friction coefficient and the viscosity of octane decrease at a comparable magnitude upon adding scCO_2,

the slip length remains more or less the same (equation 3). Therefore, the flow enhancement of octane upon adding $scCO_2$ (K_O vs. K_O_CO_2) is purely caused by the decrease in viscosity.

Conclusions

Using molecular dynamics simulations, we have studied the structural and hydrodynamic properties of multicomponent fluids (octane, $scCO_2$, and water) in both organic and inorganic nanopores. The results indicate that in an inorganic nanopore, both water and $scCO_2$ enhance the flow rate of octane. Water forms thin films near the muscovite surface, significantly reducing the friction coefficient of octane with the muscovite surface and decreasing the viscosity of octane in the nanopore. The $scCO_2$ also reduces the friction coefficient of octane with the surface and viscosity of octane in the nanopore. The reduction in both viscosity and friction coefficient upon H_2O and $scCO_2$ addition enhances the oil flow in muscovite. In the kerogen nanopore, water plays a negligible role in the friction and viscosity of octane. In contrast, $scCO_2$ reduces the friction coefficient of octane with the kerogen surface and the viscosity of octane. The oil flow enhancement is mainly due to the reduction in viscosity. These results indicate that $scCO_2$ can be used as an oil enhanced recovery additive that works for both inorganic and organic shale nanopores. Water can enhance oil flow only in inorganic shale nanopores.

Conflicts of interest

There are no conflicts to declare.

Acknowledgements

Authors thank Dr. Jacob Harvey for helpful discussion regarding the auto-correlation-function calculation. Sandia National Laboratories is a multi-mission laboratory managed and operated by National Technology and Engineering Solutions of Sandia, LLC., a wholly owned subsidiary of Honeywell International, Inc., for the U.S. Department of Energy's National Nuclear Security Administration under contract DE-NA0003525. The views expressed in this article do not necessarily represent the views of the U.S. Department of Energy or the United States Government. This research was funded by DOE's Office of Fossil Energy through National Energy Technology Laboratory (to Y. Wang).

Note and references

1. R. H. Tunuguntla, R. Y. Henley, Y. C. Yao, T. A. Pham, M. Wanunu and A. Noy, *Science*, 2017, **357**, 792-796.
2. D. Gillespie, *Nano Lett.*, 2012, **12**, 1410-1416.
3. J. C. T. Eijkel and A. van den Berg, *Microfluid. Nanofluid.*, 2005, **1**, 249-267.
4. T. A. Ho, Y. Wang, A. Ilgen, L. J. Criscenti and C. M. Tenney, *Nanoscale*, 2018, **10**, 19957-19963.
5. T. A. Ho, L. J. Criscenti and Y. F. Wang, *Sci. Rep.*, 2016, **6**, 28053.
6. T. A. Ho, D. V. Papavassiliou, L. L. Lee and A. Striolo, *Proc. Natl. Acad. Sci. U.S.A.*, 2011, **108**, 16170-16175.
7. S. Granick and S. C. Bae, *Science*, 2008, **322**, 1477-1478.
8. J. K. Holt, H. G. Park, Y. M. Wang, M. Stadermann, A. B. Artyukhin, C. P. Grigoropoulos, A. Noy and O. Bakajin, *Science*, 2006, **312**, 1034-1037.
9. B. Radha, A. Esfandiar, F. C. Wang, A. P. Rooney, K. Gopinadhan, A. Keerthi, A. Mishchenko, A. Janardanan, P. Blake, L. Fumagalli, M. Lozada-Hidalgo, S. Garaj, S. J. Haigh, I. V. Grigorieva, H. A. Wu and A. K. Geim, *Nature*, 2016, **538**, 222-225.
10. R. R. Nair, H. A. Wu, P. N. Jayaram, I. V. Grigorieva and A. K. Geim, *Science*, 2012, **335**, 442-444.
11. S. K. Kannam, B. D. Todd, J. S. Hansen and P. J. Daivis, *J. Chem. Phys.*, 2013, **138**.
12. M. Whitby, L. Cagnon, M. Thanou and N. Quirke, *Nano Lett.*, 2008, **8**, 2632-2637.
13. C. L. Wang, B. H. Wen, Y. S. Tu, R. Z. Wan and H. P. Fang, *J. Phys. Chem. C*, 2015, **119**, 11679-11684.
14. G. Tocci, L. Joly and A. Michaelides, *Nano Lett.*, 2014, **14**, 6872-6877.
15. R. S. Voronov, D. V. Papavassiliou and L. L. Lee, *Ind Eng Chem Res*, 2008, **47**, 2455-2477.
16. X. Chen, G. X. Cao, A. J. Han, V. K. Punyamurtula, L. Liu, P. J. Culligan, T. Kim and Y. Qiao, *Nano Lett.*, 2008, **8**, 2988-2992.
17. H. F. Ye, H. W. Zhang, Z. Q. Zhang and Y. G. Zheng, *Nanoscale Res Lett*, 2011, **6**, 87.
18. J. S. Babu and S. P. Sathian, *J. Chem. Phys.*, 2011, **134**, 194509
19. M. Neek-Amal, F. M. Peeters, I. V. Grigorieva and A. K. Geim, *ACS Nano*, 2016, **10**, 3685-3692.
20. L. X. Li, Y. Kazoe, K. Mawatari, Y. Sugii and T. Kitamori, *J Phys Chem Lett*, 2012, **3**, 2447-2452.
21. D. Ortiz-Young, H. C. Chiu, S. Kim, K. Voitchovsky and E. Riedo, *Nat Commun*, 2013, **4**, 2482.
22. K. L. Wu, Z. X. Chen, J. Li, X. F. Li, J. Z. Xu and X. H. Dong, *Proc. Natl. Acad. Sci. U.S.A.*, 2017, **114**, 3358-3363.
23. J. Goldsmith and C. C. Martens, *J Phys Chem Lett*, 2010, **1**, 528-535.
24. E. Secchi, S. Marbach, A. Nigues, D. Stein, A. Siria and L. Bocquet, *Nature*, 2016, **537**, 210-213.
25. Q. Xie, M. A. Alibakhshi, S. P. Jiao, Z. P. Xu, M. Hempel, J. Kong, H. G. Park and C. H. Duan, *Nat Nanotechnol*, 2018, **13**, 238-245.
26. J. A. Thomas and A. J. H. McGaughey, *Nano Lett.*, 2008, **8**, 2788-2793.
27. J. A. Thomas and A. J. H. McGaughey, *Phys. Rev. Lett.*, 2009, **102**.
28. E. Wagemann, E. Oyarzua, J. H. Walther and H. A. Zambrano, *Phys. Chem. Chem. Phys.*, 2017, **19**, 8646-8652.
29. T. A. Ho and A. Striolo, *AIChE J.*, 2015, **61**, 2993-2999.
30. T. A. Ho, Y. Wang, Y. Xiong and L. J. Criscenti, *Fuel*, 2018, **220**, 1-7.
31. T. A. Ho, Y. Wang and L. J. Criscenti, *Phys. Chem. Chem. Phys.*, 2018, **20**, 12390-12395.
32. P. Ungerer, J. Collell and M. Yiannourakou, *Energ Fuel*, 2015, **29**, 91-105.
33. R. W. Hockney and J. W. Eastwood, *Computer simulation using particles*, Taylor & Francis Group, LLC., New York, 1988.
34. Z. Q. Zhang, L. S. Yuan, Z. Liu, G. G. Cheng, H. F. Ye and J. N. Ding, *Comp Mater Sci*, 2018, **145**, 184-190.
35. S. K. Kannam, B. D. Todd, J. S. Hansen and P. J. Daivis, *J. Chem. Phys.*, 2012, **136**, 024705.

36. E. Lauga, M. P. Brenner and H. A. Stone, *Handbook of Experimental Fluid Dynamics*, Springer, New York, 2007.
37. B. Liu, R. B. Wu, A. W. K. Law, X. Q. Feng, L. C. Bai and K. Zhou, *Sci. Rep.*, 2016, **6**, 38583.
38. K. P. Travis and K. E. Gubbins, *J. Chem. Phys.*, 2000, **112**, 1984-1994.
39. D. Toton, C. D. Lorenz, N. Rompotis, N. Martsinovich and L. Kantorovich, *J Phys-Condens Mat*, 2010, **22**.
40. W. Zhu, S. J. Singer, Z. Zheng and A. T. Conlisk, *Phys. Rev. E*, 2005, **71**.
41. J. B. Freund, *J. Chem. Phys.*, 2002, **116**, 2194-2200.
42. R. Qiao and N. R. Aluru, *J. Chem. Phys.*, 2003, **118**, 4692-4701.
43. R. T. Cygan, J. J. Liang and A. G. Kalinichev, *J. Phys. Chem. B*, 2004, **108**, 1255-1266.
44. A. T. Hagler, S. Lifson and P. Dauber, *J. Am. Chem. Soc.*, 1979, **101**, 5122-5130.
45. Accelyrs, *Accelrys Software Inc.* , 2010, San Diego, CA.
46. O. Teleman, B. Jonsson and S. Engstrom, *Mol. Phys.*, 1987, **60**, 193-203.
47. J. J. Potoff and J. I. Siepmann, *AIChE J.*, 2001, **47**, 1676-1682.
48. H. Kamberaj, R. J. Low and M. P. Neal, *J. Chem. Phys.*, 2005, **122**, 224114
49. S. Nose, *Mol. Phys.*, 1984, **52**, 255-268.
50. G. J. Martyna, D. J. Tobias and M. L. Klein, *J. Chem. Phys.*, 1994, **101**, 4177-4189.
51. J. D. Miller, X. M. Wang, J. Q. Jin and K. Shrimali, *Int J Miner Process*, 2016, **156**, 62-68.
52. F. Jimenez-Angeles and A. Firoozabadi, *J. Phys. Chem. C*, 2016, **120**, 11910-11917.
53. L. Yang, Y. J. Guo and D. F. Diao, *Phys. Chem. Chem. Phys.*, 2017, **19**, 14048-14054.
54. S. T. Cui, P. T. Cummings and H. D. Cochran, *Mol. Phys.*, 1996, **88**, 1657-1664.